ORNL/SPR-2023/2951

Wireless System Development for GaN-Based Transmitters for Advanced Nuclear Reactor Environments

Tyler W. McCormick
C. Brett Witherspoon
M. Nance Ericson
N. Dianne Bull Ezell
Jack Lanza
Chandan Joishi
Hyunsoo Lee
Raymond Cao
Siddharth Rajan
F. Kyle Reed

July 2023

OAK RIDGE National Laboratory

ORNL IS MANAGED BY UT-BATTELLE LLC FOR THE US DEPARTMENT OF ENERGY

ORNL/SPR-2023/2951

Cyber Resilience and Intelligence Division
Electrification and Energy Infrastructures Division
Nuclear Energy and Fuel Cycle Division

Wireless System Development for GaN-Based Transmitters for Advanced Nuclear Reactor Environments

Tyler W. McCormick
C. Brett Witherspoon
M. Nance Ericson
N. Dianne Bull Ezell
Jack Lanza
Chandan Joishi
Hyunsoo Lee
Raymond Cao
Siddharth Rajan
F. Kyle Reed

July 2023

Prepared by
OAK RIDGE NATIONAL LABORATORY
Oak Ridge, TN 37831
managed by
UT-Battelle LLC
for the
US DEPARTMENT OF ENERGY
under contract DE-AC05-00OR22725

CONTENTS

LIST OF FIGURES

LIST OF TABLES

ABBREVIATIONS

CPS	cyber-physical systems
d-mode	depletion mode
e-mode	enhancement mode
EIRP	effective isotropic radiated power
FIR	finite impulse response
FPGA	field programmable gate array
FSK	frequency-shift keying
HEMT	high-electron-mobility transistor
I&C	instrumentation and control
IoT	internet-of-things
ISM	industrial, scientific, and medical
JFET	junction-gate field-effect transistor
LEO	low Earth orbit
LO	local oscillator
MSR	molten salt reactor
OOK	on-off keying
ORNL	Oak Ridge National Laboratory
OSU	Ohio State University
OTA	over-the-air
PWM	pulse-width modulation
rad-hard	radiation-hardened
RF	radio frequency
SDR	software-defined radio
SMR	small modular reactor
SNR	signal-to-noise ratio
SoC	system on a chip
TID	total ionizing dose
VCO	voltage-controlled oscillator
WBG	wide bandgap

ACKNOWLEDGMENTS

This work was prepared as an account of work sponsored by the U.S. Department of Energy, Office of Nuclear Energy Advanced Sensors and Instrumentation program under DOE Contract DE-NE0008591. Neither the U.S. government nor any agency thereof, nor any of their employees, makes any warranty, expressed or implied, or assumes any legal liability or responsibility for the accuracy, completeness, or usefulness, of any information, apparatus, product, or process disclosed, or represents that its use would not infringe privately owned rights. References herein to any specific commercial product, process, or service by trade name, trade mark, manufacturer, or otherwise, does not necessarily constitute or imply its endorsement, recommendation, or favoring by the U.S. Government or any agency thereof. The views and opinions of authors expressed herein do not necessarily state or reflect those of the U.S. government or any agency thereof.

ABSTRACT

The market for consumer electronics is dominated by Si-based electronics. Many Si-based complementary metal–oxide–semiconductor (CMOS) devices are reaching their limitations in terms of switching frequencies, voltages, currents, and temperatures. Furthermore, these devices are widely known to be susceptible to ionizing radiation and neutrons. Advanced nuclear reactors, especially microreactors and small modular reactors, require wireless electronics that can survive larger neutron and gamma doses than Si CMOS. Because of their size, electronics will need to be placed closer to the reactor cores, and cabling capabilities may be limited. However, GaN high-electron-mobility transistors (HEMTs) have been shown to switch faster with higher gains, and they can achieve current and voltage limits beyond traditional Si CMOS. However, they have less market maturity and have undergone less testing. These GaN HEMTs have been shown to survive ionizing radiation with little effects, but the effects of neutron radiation remain widely unknown. In this report, a wireless electronic system capable of supporting multiple radiation-hardened (rad-hard) sensors is presented. The proposed transmission scheme was designed to be simple to increase the likelihood of success in the immature GaN HEMT process and in high-radiation environments. The transmission system was tested using software-defined radios to emulate the transmission scheme before the transmitter circuitry in the GaN process was developed.

1. INTRODUCTION

Advanced reactors are poised disrupt the current energy market by providing clean energy more safely and efficiently than the current US reactor fleet. Small modular reactors (SMRs) and microreactors are intended to be small, compact reactors that will be field deployable and autonomous. However, the electronics required to control and operate these reactors may need to be placed in locations of intense heat and radiation—both ionizing and neutron. Furthermore, reducing cabling requirements may be necessary in the smaller geometries of SMRs and microreactors, requiring wireless and through-wall transmission. Even in large-scale advanced reactors such as molten salt reactors (MSRs), reducing cabling with easily deployable wireless sensors will enable new capabilities for instrumentation and control (I&C).

Advanced wireless technologies have the potential to enable a new range of capabilities for I&C in current and next-generation nuclear reactors. The flexibility of wireless sensing allows for easily deployable and replaceable sensors and instrumentation. This promising technology should enhance nuclear facility safety and operations. The ever-increasing amount of analog sensing data from internet-of-things (IoT) and cyber-physical systems (CPS) drives the development of new data-driven algorithms to transform raw sensor data into useful and actionable information. The ability to economically deploy wireless sensors equipped with radiation-hardened (rad-hard) electronics allows the nuclear industry to leverage these emerging intelligent sensing technologies to better understand and control plant operations and processes. Furthermore, the mobility provided by wireless sensing and communications coupled with rad-hard electronics opens up new application domains, including the use of mobile drones and robots for automated maintenance, condition monitoring, and nuclear-disaster response.

To enable wireless applications, suitable rad-hard electronics for nuclear reactor environments must be investigated. The present market of rad-hard electronics is dominated by low Earth orbit (LEO) and space-exploration missions, which have lower total ionizing doses (TIDs), much higher particle energies, and little to no neutrons (unless powered or propelled by an onboard nuclear reactor). In these applications, Si CMOSs are the most common form of electronics. However, they are susceptible to charge trapping and displacement damages. With proper modern design techniques, Si CMOS can withstand ~1 MGy but only

10^{14} n/cm^2 [1, 2, 3, 4, 5].

The radiation survivability of commercially available Si CMOS depends on the neutron fluences required to operate near or in the core of advanced reactors. However, wide bandgap (WBG)-based semiconductors such as SiC and GaN are promising semiconductor candidates to extend the neutron tolerance of electronic circuitry owing to their doping [6, 7]. The SiC junction-gate field-effect transistors (JFETs) can withstand $\geq$1 MGy and 10^{16} n/cm^2. However, modern processes require $\pm$24 V power, and they switch slower than GaN high-electron-mobility transistors (HEMTs), making them less ideal for low-voltage wireless applications. The GaN HEMTs are of particular interest: they are inherently insensitive to ionizing radiation because they lack a gate insulator for both enhancement mode (e-mode) and depletion mode (d-mode) device topologies [7], but their neutron tolerance remains unverified.

To enable wireless sensing for near- or in-core environments, researchers at the US Department of Energy's Oak Ridge National Laboratory (ORNL) and Ohio State University (OSU) are investigating potentially rad-hard GaN HEMT-based wireless transmitter circuitry [8]. This report details further development on the wireless sensor transmitters presented in [8] by implementing the pulse-width modulation (PWM)-based binary transmission and modulation scheme using a software-defined radio (SDR) test bed consisting of a set of ADALM-PLUTOs (Analog Devices Inc.; Wilmington, Massachusetts) to emulate the proposed GaN-based transmitter circuits and base station hub.

2. ROBUST COMMUNICATIONS TEST BED

To evaluate the efficacy of the modulation and encoding schemes presented in [8], a software framework and hardware platform were combined to form a robust communications test bed. The chosen modulation and encoding schemes were then implemented on the robust communications test bed to emulate the GaN transmitter and SDR receiver depicted in [8]. The following sections describe the chosen software framework, hardware platform, modulation and encoding schemes, as well as the emulated transceiver architecture for two transmitters and a single receiver.

2.1 SOFTWARE FRAMEWORK

Due to its maturity and broad compatibility with a wide range of SDR platforms, GNU Radio was chosen as the software framework for the robust communications test bed. GNU Radio is a toolkit written in Python/C++ that simplifies SDR development and integration. GNU Radio simplifies development and integration by implementing popular signal processing algorithms and radio frequency (RF) hardware interface modules in the form of ready-made blocks [9]. Additionally, the resulting system can be visualized such that the data flow of the system can be easily understood.

2.2 HARDWARE PLATFORM

To accompany the software framework, the ADALM-PLUTO SDR was chosen as the hardware platform due to to its low cost and its wide hardware and software compatibility. This platform includes an Analog Devices AD9364 RF transceiver and a Xilinx Zynq-7000S field programmable gate array (FPGA) system on a chip (SoC) processing system [8]. The SoC processing system consists of an ARM Cortex-A8 processor and Artix-7 programmable logic fabric [8].

2.3 MODULATION AND ENCODING METHODS

In its simplest form, digital communications involves information that must be sent from a transmitter to receiver. To transmit this information, often the information is converted to a different form and then changed again such that the information is suitable for transmission over a channel. These two steps are known as encoding and modulation, respectively. While it is often best to choose the most efficient or fast encoding and modulation methods, the harsh environment of the transmitter imposes a set of requirements which rules out most forms of modulation and encoding. This section will briefly discuss unsuitable methods of modulation and encoding as well as the chosen methods for this project.

2.3.1 Modulation

In digital communications, a receiver must estimate a sequence of discrete transmitted symbols in order to recreate the the initially transmitted signal [8]. The received signal often contains noise and other factors which serve to corrupt the transmitted signal. In the case of this project, while the received signal will likely contain noise, the main corrupting factor will likely be in the form of radiation-induced frequency variations, caused by the location of the transmitter. Therefore, a resilient modulation method should be chosen in order to best combat these radiation-induced frequency variations. For this project, a binary modulation method was chosen. Binary modulation was chosen because it is simple and exhibits better resilience to frequency variations compared to multi-level modulation methods [8].

There are many existing binary digital modulation methods. However, many of them are unsuitable due to the strict requirements imposed by the large radiation-induced frequency variations. For example on-off keying (OOK), while simple to implement, would require careful gain control and thresholding, and is therefore unsuitable [8]. Chirp keying is another binary modulation method. While this method would result in a signal-to-noise ratio (SNR) improvement, this method is unsuitable because of the complexity required to implement a chirp transmitter. Ultimately, the modulation method chosen for this project is frequency-shift keying (FSK). FSK is a modulation method whereby information is transmitted by a shift in frequency in response to the information being transmitted [8]. While less spectrally efficient than chirp keying and more complex than OOK, its inherent ability to resist large frequency variations makes FSK an ideal choice for this particular application.

2.3.2 Encoding

In digital communications, information is often converted into a format that is compatible with a chosen modulation method. FSK modulation was chosen, so the analog values from the sensors must first be encoded into a bipolar waveform before the data can be modulated and then transmitted.

Two methods of encoding analog values into a bipolar waveform are pulse density encoding and pulse-width encoding or PWM. Pulse density encoding encodes and analog value as a string of bipolar pulses, where the frequency of the pulses is directly proportional to the analog value [8]. PWM encodes an analog value as a square wave, where the duty-cycle of the square wave is directly proportional to the analog value being encoded. For this project, PWM encoding was chosen because this project involves a new process node, and PWM encoding is simpler to implement than pulse density encoding.

3. IMPLEMENTATION

The robust communications test bed described in Section 2. emulates two voltage sensors transmitting PWM-encoded and FSK-modulated values, with a single receiver demodulating and recovering both values. As described in Section 2., the test bed was implemented using GNU Radio as the software framework and ADALM-PLUTO as the SDR hardware platform. This section describes the various parts of the software and hardware implementation in GNU Radio and how these parts interact.

3.1 HARDWARE CONFIGURATION

To properly use the SDR platform, the hardware must be connected and configured. GNU Radio abstracts most of the minutia of configuring an SDR, but it leaves the choice of many configurable options to the user. In this project, the sample rate f_s and the local oscillator (LO) frequency were varied. For this test bed, the sample rate was set to 1.92 MHz and the LO frequency was set to 915 MHz. The sample rate was chosen because it is well below the practical sample rate limit of 4–5 MHz, as detailed by [10]. The LO frequency was set to 915 MHz because that frequency falls near the middle of one of the unlicensed industrial, scientific, and medical (ISM) frequency bands, and thus no licences were required to operate within this band if the maximum effective isotropic radiated power (EIRP) is no greater than 4 W, as explained by [11].

3.2 SIGNAL ENCODING AND MODULATION

Accurately testing whether the chosen encoding and modulation methods are suitable for transmitting sensor values over-the-air (OTA) requires simulating the entire transmission chain. Figure 1 is a block diagram of the entire transmission chain for the chosen encoding and modulation methods. This section demonstrates how analog voltage was emulated, how this voltage was encoded, and how this encoded signal was modulated.

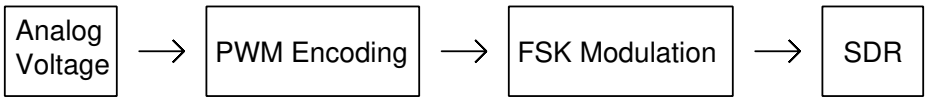

Figure 1. Block diagram of transmission chain.

3.2.1 Analog Voltage Emulation

To emulate the two analog sensor values, a simple range block of 0 to 1 V with steps of 1 mV was used. Figure 2 depicts the block used along with its parameters.

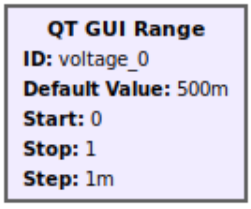

Figure 2. Range block used to emulate analog sensor value.

This range block can be changed in real time to simulate changing sensor values while the test bed is running. Because two sensors transmitting simultaneously were emulated, a second emulated analog voltage was added for the second sensor.

3.2.2 PWM Encoding

Following the range block, the encoding of the analog sensor value using PWM was emulated using a vector source block. In GNU Radio, the vector source block can be used to create a stream of repeating binary values. To create a square wave with a duty cycle directly proportional to the analog sensor value provided by the range block, the vector source block was programmed to generate a stream of binary values using Eq. (1):

$$f[x] = \begin{cases} 1 & n \in [0, 1, ..., \lfloor N \cdot (1 - v) \rfloor] \\ 0 & o.w. \end{cases}, \tag{1}$$

where N is the total number of elements chosen for the repeating stream, and v is the emulated analog voltage. In GNU Radio, the frequency at which the vector source block repeats the generated stream is inversely proportional to the total number of elements in the stream. The period of the repeated stream can be computed via Eq. (2):

$$T_{pwm} = \frac{N}{f_s}, \tag{2}$$

where f_s is the sample rate set in GNU radio, and N is the total number of elements in the stream. For the case with a sample rate of 1.92 MHz, a period of 0.0002 provided the best results, so the total number of elements in the stream was chosen to be 384. Figure 3 illustrates creating the stream represented by Eq. (1). A second vector source block of the same length was added in order to encode the second emulated sensor value.

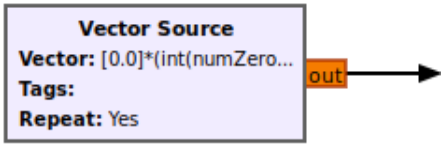

Figure 3. Vector source block used to encode the analog sensor value.

3.2.3 FSK Modulation

Once the analog sensor value was encoded into a PWM signal, an FSK modulator must be created. As shown in [12], a voltage-controlled oscillator (VCO) can be used to create an FSK modulated signal that is simple to demodulate. The VCO block produces a sinusoidal waveform with a frequency that is directly proportional to the input value and the maximum frequency of the VCO, which is configured by setting the sensitivity parameter. The frequency of the sinusoidal output of the VCO can be computed using Eq. (3:

$$f_{\text{out}} = \frac{v_{\text{in}}}{v_{\text{max}}} \cdot f_{\text{max}}, \tag{3}$$

where v_{in} is the input value, v_{max} is the maximum input value possible, and f_{max} is the maximum frequency produced by the VCO.

Correctly configuring the VCO block requires specifying its sensitivity, sample rate, and the amplitude of the output waveform. The sample rate was set to 1.92 MHz, and the amplitude was set to 0.5. As demonstrated by [13], the sensitivity of the VCO must be set according to Eq. (4):

$$\mu = \frac{2\pi f_{\text{max}}}{v_{\text{max}}}, \tag{4}$$

where f_{max} is the maximum frequency the VCO should ever generate, and v_{max} is the maximum voltage expected at the input. For this test bed, because the PWM-encoded signal contains only binary values, the maximum voltage input will always be 1 V. Setting the maximum frequency only requires choosing a frequency greater than the two FSK frequencies that will be generated by the VCO. For any generic FSK modulator, the VCO must generate two frequencies: one frequency represents the transmission of a 0, and the other represents the transmission of a 1. These two frequencies can be denoted as fsk_0 and fsk_1, respectively. The maximum frequency generated by the VCO can then computed using Eq. (5):

$$f_{\text{max}} = \text{fsk}_1 + 0.1 \text{ MHz}, \tag{5}$$

where fsk_1 is the frequency chosen to represent the transmission of a 1, and 0.1 MHz is an arbitrarily chosen buffer.

Although the VCO has been properly configured, it will not yet produce the desired FSK frequencies of fsk_0 and fsk_1 for inputs of 0 and 1. To produce a frequency of fsk_0 when the input is 0, an offset proportional to the desired frequency and the maximum frequency of the VCO must be added to the input, as shown in [12]. This offset can be computed using Eq. (6):

$$\alpha = \frac{\text{fsk}_0}{f_{\text{max}}}, \tag{6}$$

where fsk_0 is the frequency chosen for the transmission of a 0, and f_{max} is the maximum frequency of the sinusoidal waveform that the VCO can generate.

In addition to this offset α, a scaling factor must be multiplied by the input before the offset is added to the input. This scaling factor can be computed using Eq. (7):

$$\beta = \frac{\text{fsk}_1}{f_{\text{max}}} - \alpha, \tag{7}$$

where fsk_1 is the frequency chosen to represent the transmission of a 1, f_{max} is the maximum frequency of the sinusoidal waveform that the VCO can generate, and α is the previously computed VCO offset.

When this scaling factor is multiplied by the input before the addition of the offset, raw inputs will produce a modified input to the VCO, which can be computed via Eq. (8):

$$v_m = (\beta \cdot v_{\text{in}}) + \alpha. \tag{8}$$

To compute these values for the first emulated sensor in the test bed, the two FSK frequencies were chosen to be $\text{fsk}_0 = 0.1$ MHz and $\text{fsk}_1 = 0.2$ MHz. Using $\text{fsk}_1 = 0.2$ MHz, the maximum frequency $f_{\max}$ can be computed using Eq. (5), which yields

$$f_{\max} = 0.2 \text{ MHz} + 0.1 \text{ MHz} = 0.3 \text{ MHz}. \tag{9}$$

The maximum frequency of the VCO, $f_{\max}$, can then be used to compute the sensitivity of the VCO using Eq. (4), which yields

$$\mu = \frac{2\pi(0.3 \times 10^6)}{1} \approx 1.89 \times 10^6. \tag{10}$$

The VCO offset, α, can then be computed using Eq. (6), which yields

$$\alpha = \frac{0.1 \text{ MHz}}{0.3 \text{ MHz}} \approx 0.33. \tag{11}$$

The offset can then be used to compute the VCO scaling factor, β, which, when computed using Eq. (7) yields

$$\beta = \frac{0.2 \text{ MHz}}{0.3 \text{ MHz}} - 0.33 \approx 0.33. \tag{12}$$

Using the previously computed values for β and α and a raw input of 0 yields the following modified input:

$$v_m = (0 \cdot 0.33) + 0.33 = 0 + 0.33 = 0.33, \tag{13}$$

which, when used in Eq. (3), yields the desired frequency of 0.1 MHz for an input of 0:

$$f_{\text{out}} = \frac{0.33}{1} \cdot 0.3 \text{ MHz} \approx 0.1 \text{ MHz}. \tag{14}$$

Using Eq. (8) for an input of 1 results the following modified input:

$$v_m = (1 \cdot 0.33) + 0.33 = 0.33 + 0.33 = 0.66, \tag{15}$$

which, when used in Eq. (3), produces the desired frequency of 0.2 MHz for an input of 1:

$$f_{\text{out}} = \frac{0.66}{1} \cdot 0.3 \text{ MHz} \approx 0.2 \text{ MHz}. \tag{16}$$

The process for computing the offset, scaling factor, and sensitivity for the FSK modulator of the second emulated sensor was repeated for FSK frequencies of $\text{fsk}_0 = 0.3$ MHz and $\text{fsk}_1 = 0.4$ MHz, as well as a maximum frequency of $f_{\max} = 0.5$ MHz. Repeating this process resulted in a sensitivity of approximately

3.14×10^6 (Eq. [4]), an offset of 0.6 (Eq. [6]), and a scaling factor of 0.2 (Eq. [7]). These values were then used to create the FSK modulation chain for the second emulated sensor.

To implement the scaling factor and offset in GNU Radio, a multiply block and an add constant block were used. These blocks multiply and add a constant value to their inputs, respectively. The complete FSK modulation chain for the first emulated sensor as implemented in GNU Radio is pictured in Figure 4.

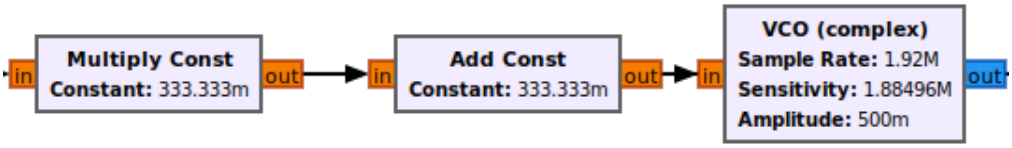

Figure 4. Complete FSK modulation chain for first emulated sensor.

To complete the entire emulated transmission chain, the PWM-encoded analog voltage for both emulated sensors was connected to the input of the FSK modulation chain, as illustrated in Figure 5.

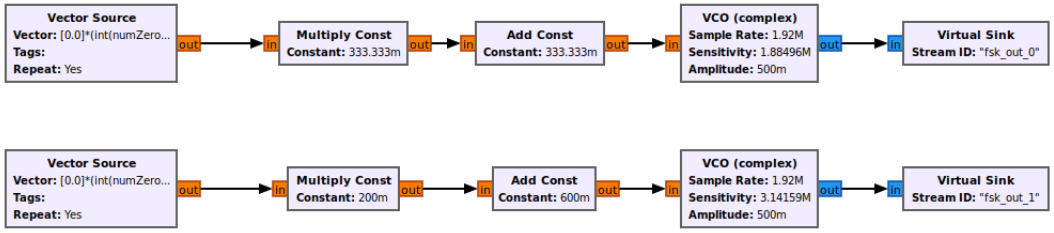

Figure 5. Complete transmission chain for both emulated sensors.

The two "Virtual Sink" blocks pictured at the end of the chain serve only to connect the outputs without cluttering the flow graph and have no effect on the transmission process.

The outputs of both transmission chains were then connected to two separate ADALM-PLUTO SDRs so that they can each be transmitted, as pictured in Figure 6.

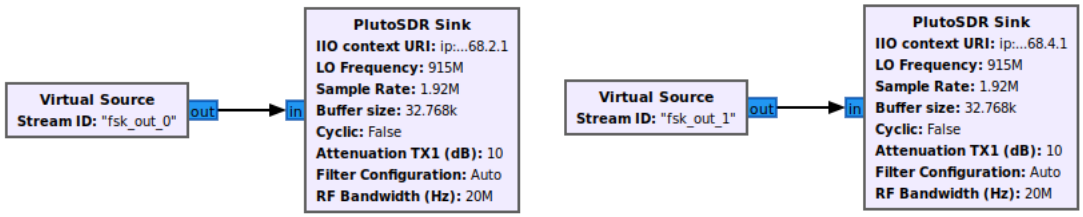

Figure 6. Transmission interfaces in GNU Radio for each emulated sensor.

In GNU Radio, an ADALM-PLUTO SDR can be used to transmit samples by connecting the desired output to the input of a PlutoSDR sink block. The actual low-level transmission process is abstracted by the sink block, which requires only a few parameters. For this test bed, all parameters were the default options, except for the LO frequencies and sample rates, which were set to 915 MHz and 1.92 MHz, respectively.

3.3 SIGNAL DECODING AND DEMODULATION

To reconstruct the two emulated analog sensor values, a single SDR must be used to receive the two modulated sensor signals, where each signal is demodulated and then decoded to reproduce the original emulated analog voltage. Figure 7 shows a block diagram of the entire receive chain.

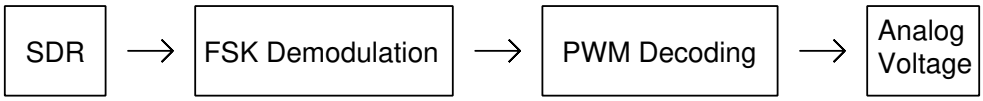

Figure 7. Block diagram of receive chain.

This section demonstrates how the modulated signals are received, demodulated, and decoded to produce the two emulated analog sensor values.

3.3.1 Receiving the Signal

To receive the modulated signals produced by the transmission chains of the two emulated sensors, a PlutoSDR source block was used. Similar to a sink block, a source block abstracts the procedure required for receiving a signal in GNU Radio. Like the sink blocks, the default parameter choices were unchanged, except for the LO frequency and the sample rate. Figure 8 depicts how one SDR was used to receive the modulated signals produced by the transmission chains of the two emulated sensors.

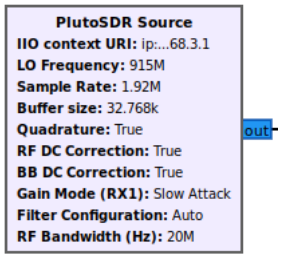

Figure 8. Receive interface in GNU Radio for emulated sensor signals.

3.3.2 Demodulation

To demodulate an FSK modulated signal, the band containing its two frequencies must be searched, and the demodulator decides which frequency is more likely to be present at the decision time [14]. GNU Radio already contains a built-in demodulation block, known as the quadrature demodulation block. As demonstrated by [15], the quadrature demodulation block expects the FSK band to be shifted down to baseband, with the zero frequency on the left and the one frequency on the right. To shift each emulated sensor's FSK band, a frequency-translating finite impulse response (FIR) filter block was used. As demonstrated by [16], this block can shift a bandwidth-limited portion of the spectrum down to baseband while applying an FIR filter with optional decimation to minimize nearby noise and reduce processing time. For the block to work correctly, center frequency, sample rate, filter taps, and decimation factor must be specified.

For each emulated sensor, the sample rate and decimation factor were set to 1.92 MHz and 1, respectively. Each band's center frequency was computed using

$$f_c = f_{lo} + f_{cb} + f_{off}, \tag{17}$$

where f_{lo} is the frequency of the LO, f_{cb} is the center frequency of the baseband FSK signal for the specific emulated sensor, and f_{off} is an experimentally determined frequency offset. For both sensors, the LO frequency is 915 MHz. Because each band occupies a different portion of the spectrum, the center frequency of the baseband FSK signal must be computed individually using

$$f_{cb} = \text{fsk}_0 + \frac{\text{fsk}_1 - \text{fsk}_0}{2}, \tag{18}$$

where fsk_0 is the frequency representing a 0, and fsk_1 is the frequency representing a 1. Using values of 0.1 MHz and 0.2 MHz for each frequency, respectively, yields a baseband center frequency of 0.15 MHz:

$$f_{cb} = 0.1 \text{ MHz} + \frac{0.2 \text{ MHz} - 0.1\text{MHz}}{2} = 0.1 \text{ MHz} + 0.05 \text{ MHz} = 0.15 \text{ MHz}. \tag{19}$$

Using this center baseband frequency of 0.15 MHz, a LO frequency of 915 MHz, and a frequency offset of 0.844 MHz yields 915.994 MHz as the center frequency of the frequency-translating FIR filter block:

$$f_{c,1} = 915 \text{ MHz} + 0.15 \text{ MHz} + 0.844 \text{ MHz} = 915.994 \text{ MHz}. \tag{20}$$

This process was repeated for the second emulated sensor, yielding 916.194 MHz as the center frequency of the frequency-translating FIR filter block:

$$f_{c,2} = 915 \text{ MHz} + 0.35 \text{ MHz} + 0.844 \text{ MHz} = 916.194 \text{ MHz}. \tag{21}$$

The final parameter for each filter is the optional FIR filter, which reduces noise by filtering the downshifted signal. In order to filter the downshifted signal, the taps of an FIR filter must be specified. The frequency-translating FIR filter block accepts taps computed external to GNU Radio or taps computed internally using GNU Radio functions. For simplicity, rather than precomputing the filter taps, an included GNU Radio low-pass filter designer function computed the filter taps on the fly. The function can be utilized by calling

```
firdes.low_pass(1.0,fs,fstop,bw),
```

as shown in [16], where fs is the sample rate, fstop the frequency at which the passband should begin to transition into the stop band, and bw is how wide the transition period should be, which is specified in hertz. For both emulated sensors, the stop frequency of the low-pass FIR filter was computed using

$$f_{\text{stop}} = \text{fsk}_1 - \text{fsk}_0, \tag{22}$$

where fsk_0 is the frequency representing a 0 and fsk_1 is the frequency representing a 1. The transition bandwidth was arbitrarily specified to 10 kHz. Therefore, the taps for the low-pass filter for each emulated sensor were specified using the following line:

```
firdes.low_pass(1.0,1920000,100000,10000).
```

Once the band containing each FSK signal was shifted down to baseband and filtered, a simple squelch function was applied to the output to eliminate any signals less than a specified decibel level. For each sensor, signals less than 70 dB were removed.

The output of the squelch function was then passed to the quadrature demodulation block. The quadrature demodulation block acts as an envelope detector, outputting floating-point values greater to or less than one, depending on which signal has more strength, or zero if each signal is equally strong [15]. This block has only a single parameter, a gain value, which can be computed using

$$\text{gain} = \frac{f_s}{2\pi(\text{fsk}_1 - \text{fsk}_0)}. \tag{23}$$

Computing this gain value yields the following value for each emulated sensor:

$$\text{gain} = \frac{1.92\ \text{MHz}}{2\pi(0.1)\ \text{MHz}} \approx 3.056. \tag{24}$$

The output of the quadrature demodulator was then simplified using a binary slicer block, which essentially converts floating-point binary values to true binary values [17]. Combining the frequency-translating FIR filter block, squelch function, quadrature demodulation block, and binary slicer block produced the entire FSK demodulation chain for each emulated sensor, as shown in Figure 9.

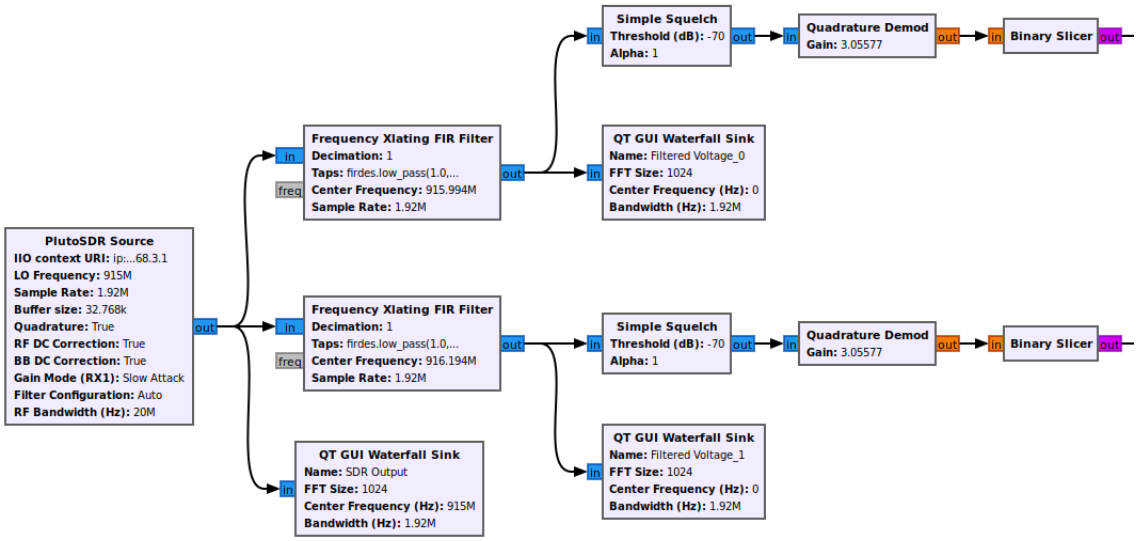

Figure 9. FSK demodulation chain for both emulated sensor signals.

3.3.3 PWM Decoding

Once each emulated sensor value has been received and demodulated, the emulated analog voltage value can be decoded and recovered from the demodulated signal. To decode the original emulated analog voltage, a simple low-pass FIR filter can be applied to the output of the demodulated signal [8][18]. Therefore, a low-pass filter block was used to decode the demodulated signal. The only parameters changed from the

default values of the low-pass signal block were the sample rate, which was set to 1.92 MHz, the cutoff frequency, which was specified as 100 Hz, and the transition width, which was specified as 50 Hz. The complete low-pass filter decoder for each emulated sensor is pictured in Figure 10, along with a simple data-type converter to convert the output of the binary slicer back to a floating-point value. The output of this chain is thus a recovered version of the original emulated analog voltage.

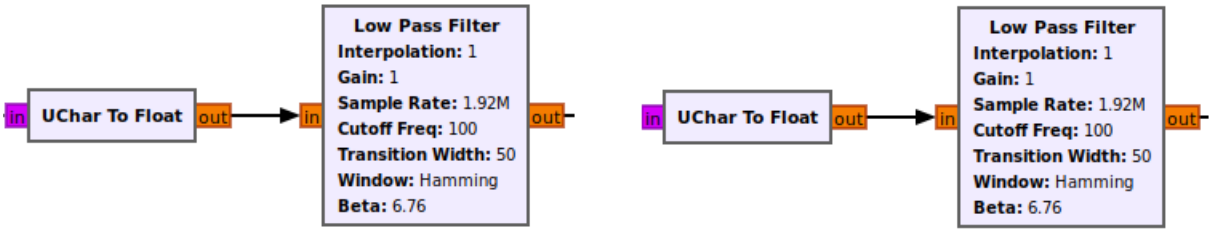

Figure 10. Low-pass FIR filter to decode the PWM signal.

4. RESULTS

After implementing the robust communications test bed described in Section 2., the test bed was tested using a simple OTA configuration. This configuration, pictured in Figure 11, uses three ADALM-PLUTO SDRs connected to the same host.

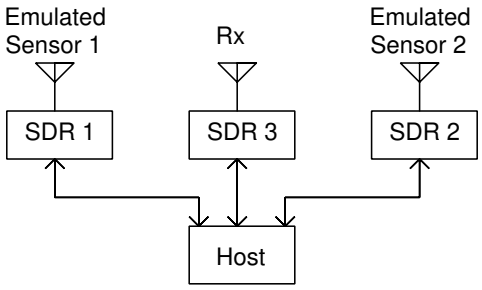

Figure 11. SDR configuration for robust communications test bed.

Additionally, each SDR was connected to the host using a USB 2.0 interface. Although each radio is connected to the same host machine, no information is exchanged between radios over the USB interface, only over the transmit and receive ports of the radios themselves. This setup was employed to simplify the experimental tests: only a single host was required, instead of one host per radio. This section describes the tests that were performed as well as the results of those tests.

4.1 EXPERIMENTAL SETUP

In addition to the configuration pictured in Figure 11, 30 dB attentuators were added to the transmit ports of each emulated sensor SDRs. These attentuators were added to keep transmitted signal at low levels so as to not interfere with other devices sharing the 900 MHz band of the ISM spectrum. For additional attenuation, 10 dB of software attenuation were also added.

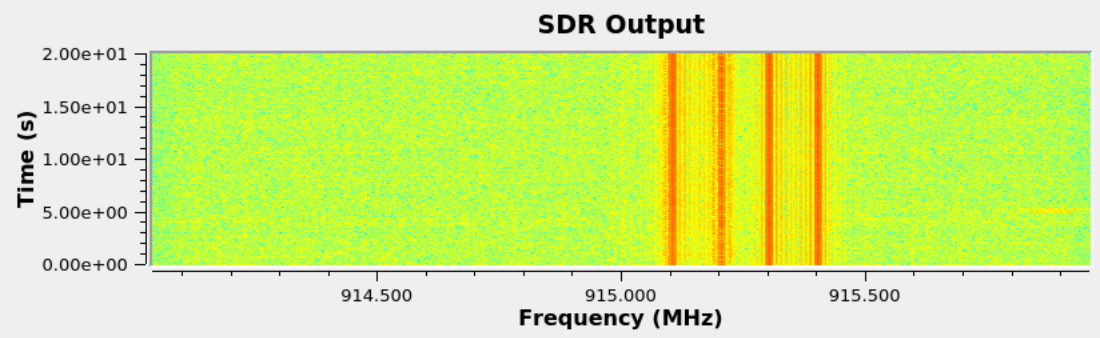

Figure 12. Waterfall plot of raw SDR output for Test 1.

Finally, this series of tests was performed in a small office: each radio was approximately 1 m away from the other two radios, such that the resulting formation was approximately triangular.

4.2 EXPERIMENTAL TESTS

Using the hardware configuration described in Section 4.1, three tests were performed. The three tests were designed to test a variety of sensor values for each emulated sensor. These tests are enumerated in Table 1.

Table 1. Voltage values of each sensor for each test

Test #	Sensor 1 (V)	Sensor 2 (V)
1	0.5	0.5
2	0.5	0.85
3	0.15	0.85

4.2.1 Test 1

Test 1, listed in Table 1, investigated the performance of both emulated sensors at the same emulated voltage level of 0.5 V. Once both emulated sensors were set to 0.5 V, the test was left running for 60 s. After this time had elapsed, waterfall plots were recorded for both shifted FSK signals as well as the raw output of the SDR. In Figure 12, the raw output of the SDR clearly shows both FSK signals modulated at the chosen LO frequency of 915 MHz. The plots for both FSK signals, pictured in Figures 13 and 14, demonstrate how the frequency-translating FIR filter shifts each emulated sensor's FSK signal down to baseband.

In addition to the three waterfall plots, a historical plot of the relative error of both emulated sensor's recovered voltages was also captured, as shown in Figure 15. The error plot in Figure 15 demonstrates that the relative error for both sensors' recovered voltages remains very low throughout the test.

4.2.2 Test 2

Immediately following Test 1, the emulated voltage of Sensor 2 was changed to 0.85 V, as depicted in Table 1. Unlike Test 1, instead of waiting 60 s, the waterfall and error plots were recorded after 20 s had elapsed to demonstrate the transition period for each transmitter. After this time had elapsed, waterfall plots were recorded for the raw output of the SDR as well as both shifted FSK signals, which are shown in Figures

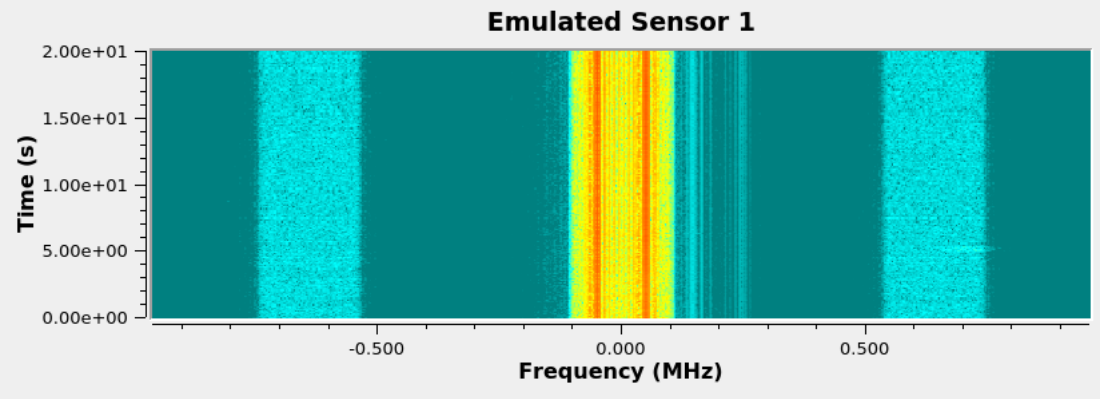

Figure 13. Waterfall plot of emulated Sensor 1 baseband FSK signal.

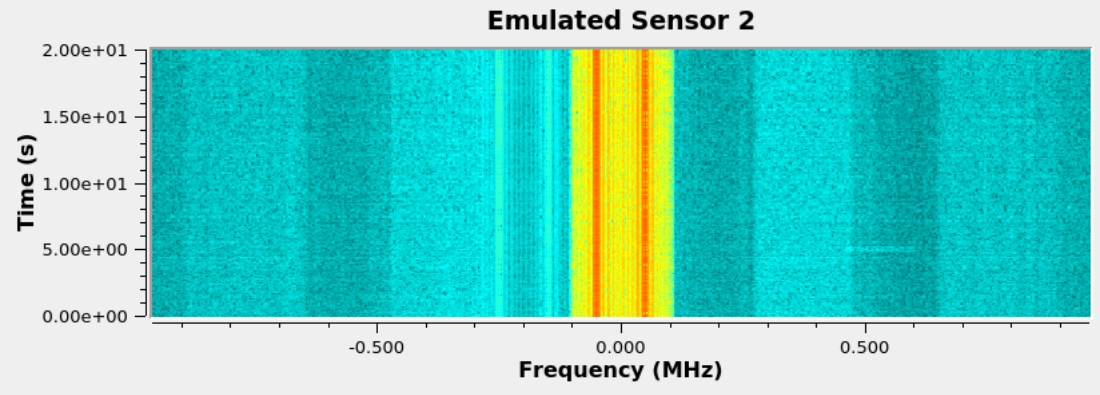

Figure 14. Waterfall plot of emulated Sensor 2 baseband FSK signal.

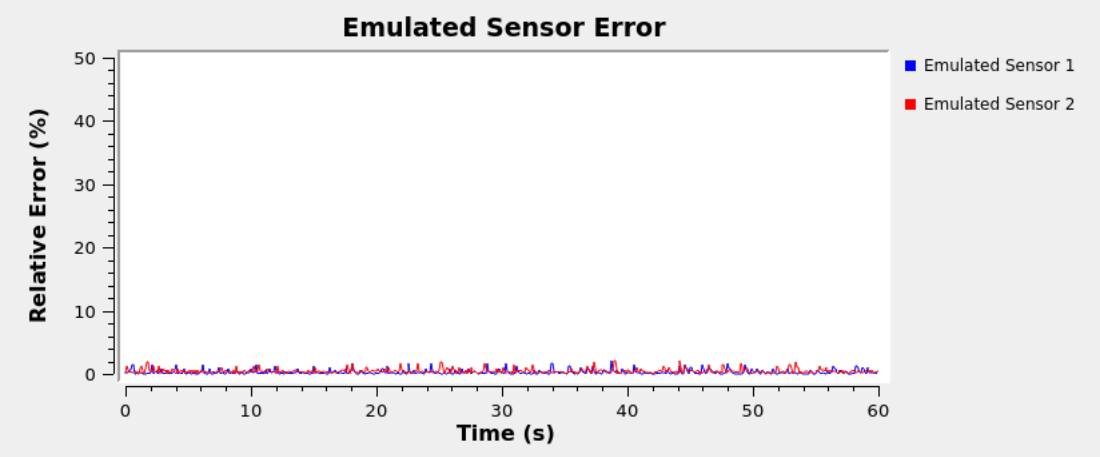

Figure 15. Historical plot (60 s) of relative error of each sensor's recovered voltage recorded during Test 1.

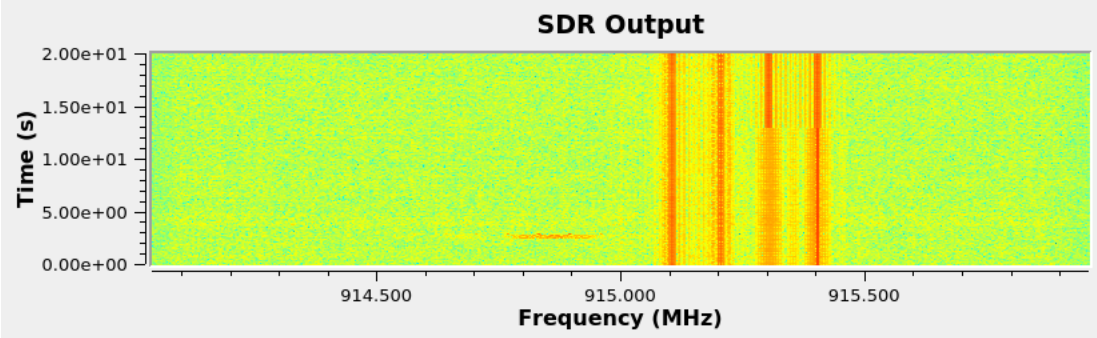

Figure 16. Waterfall plot of raw SDR output for Test 2.

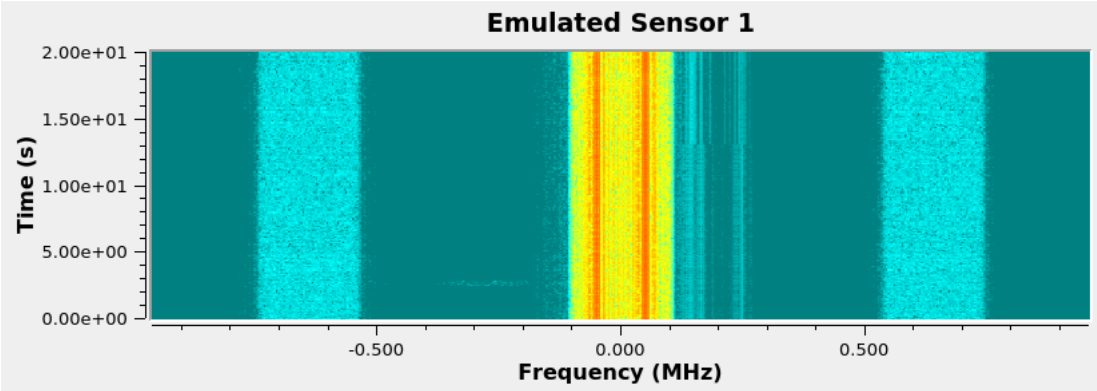

Figure 17. Waterfall plot of emulated Sensor 1's baseband FSK signal during Test 2.

16, 17, and 18, respectively. As demonstrated in Figures 16 and 18, the density of emulated Sensor 2's FSK signal changes once the emulated voltage was altered.

In addition to the three waterfall plots, a historical plot of the relative error of both emulated sensor's recovered voltages was also captured, as shown in Figure 19. The error plot in Figure 19 demonstrates that the relative error for Sensor 2's recovered voltage increases sharply after the change it made but settles back down to around 0% within around 5 s.

4.2.3 Test 3

Immediately following Test 2, the emulated voltage of Sensor 1 was changed to 0.15 V, as depicted in Table 1. Like Test 2, the plots for Test 3 were captured after 20 s. After this time had elapsed, waterfall plots were recorded for the raw output of the SDR as well as both shifted FSK signals, which are shown in Figures 20, 21, and 22, respectively. As demonstrated in Figures 20 and 21, the density of emulated Sensor 1's FSK signal changes once the emulated voltage was altered.

In addition to the three waterfall plots, a historical plot of the relative error of both emulated sensor's recovered voltages was also captured, as shown in Figure 23. The error plot in Figure 23 demonstrates that the relative error for Sensor 1's recovered voltage increases sharply after the change it made but settles back down to around 0% within around 5 s.

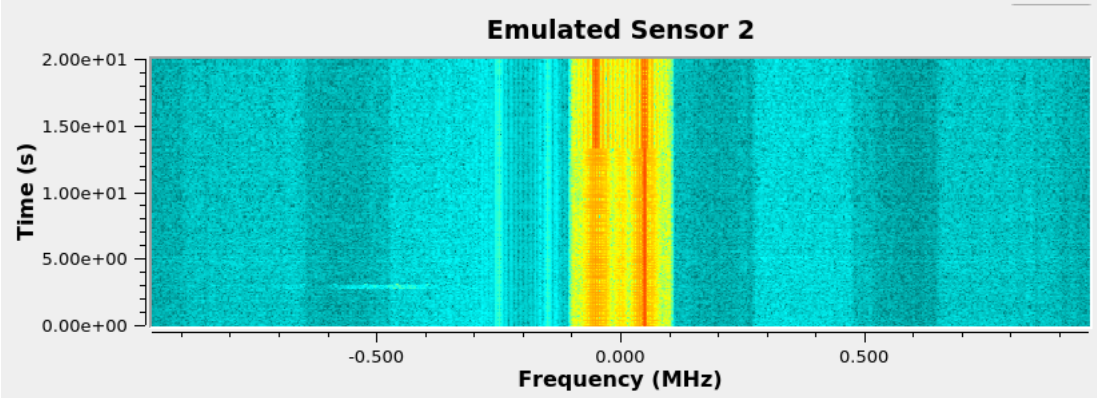

Figure 18. Waterfall plot of emulated Sensor 2's baseband FSK signal during Test 2.

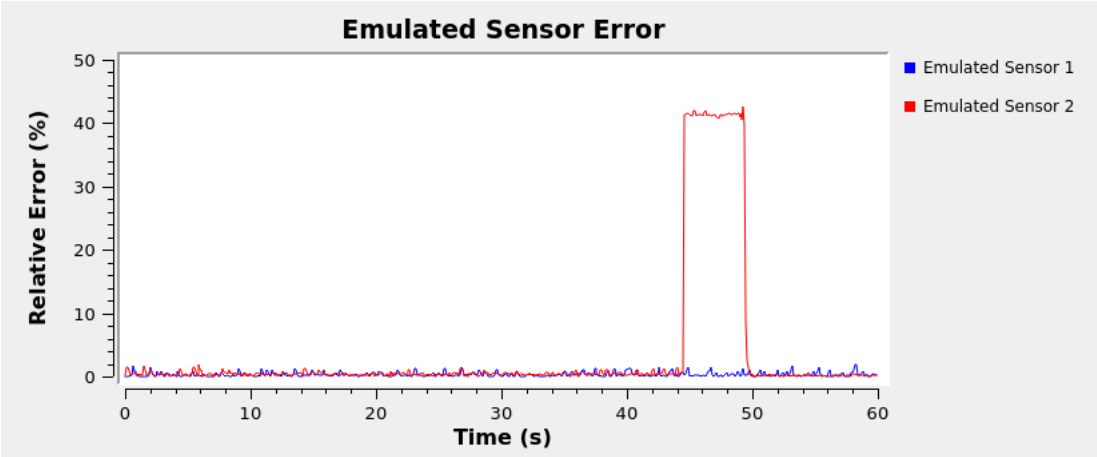

Figure 19. Historical plot (60 s) of relative error of each sensor's recovered voltage recorded during Test 2.

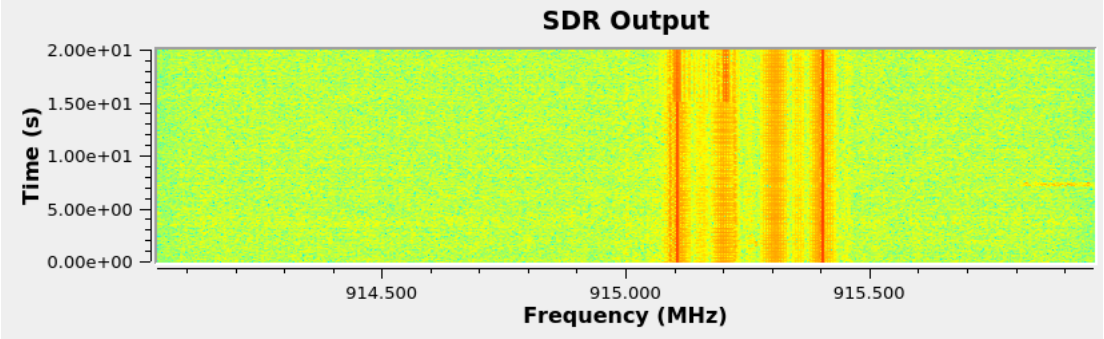

Figure 20. Waterfall plot of raw SDR output for Test 3.

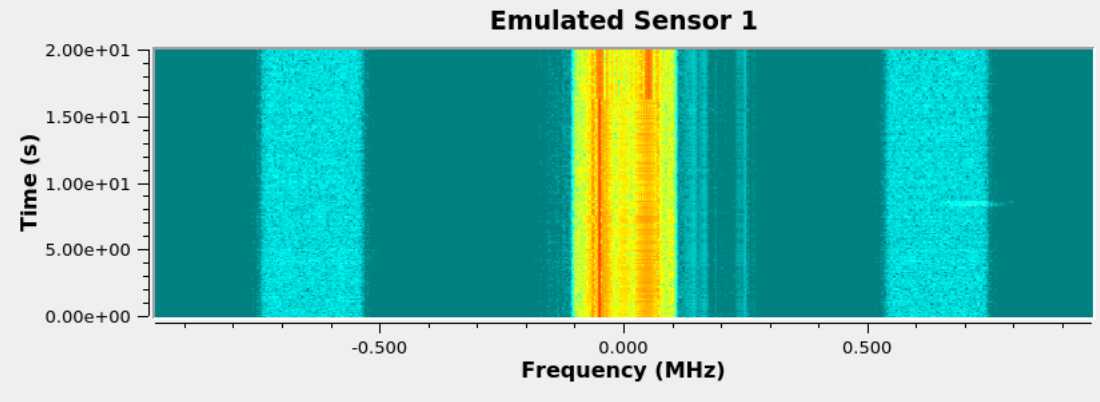

Figure 21. Waterfall plot of emulated Sensor 1's baseband FSK signal during Test 3.

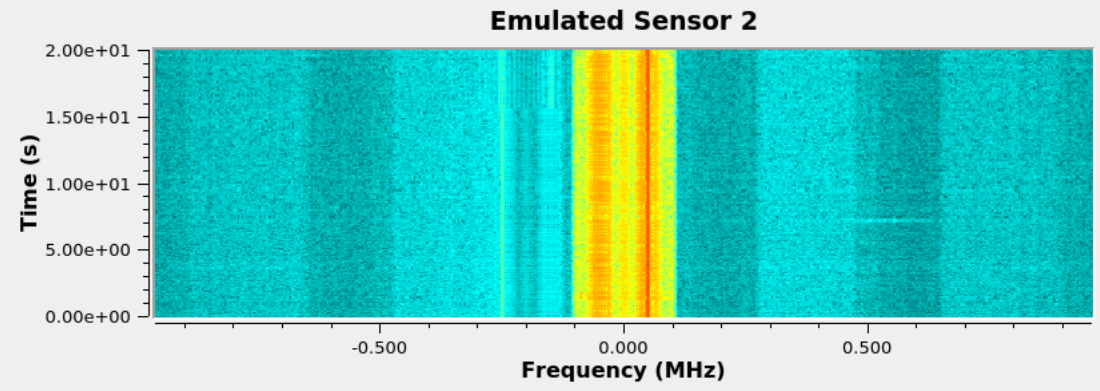

Figure 22. Waterfall plot of emulated Sensor 2's baseband FSK signal during Test 3.

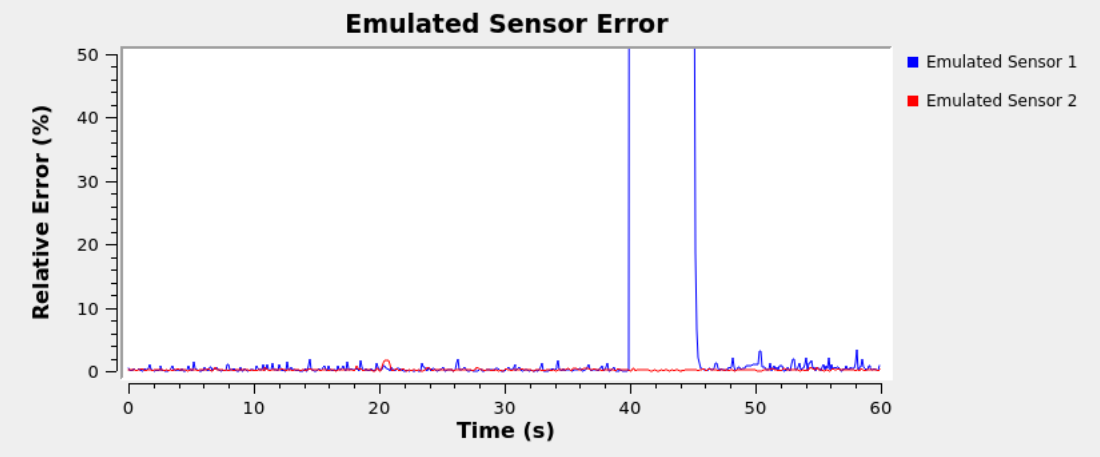

Figure 23. Historical plot (60 s) of relative error of each sensor's recovered voltage recorded during Test 3.

5. CONCLUSION

In harsh advanced nuclear reactor environments, electronics and sensors used for wireless monitoring must endure large TID and fluences throughout their lifetimes. Near- or in-core placement of electronics requires considerations beyond the scope of typical space-grade rad-hard electronics. To increase the radiation tolerance of electronics required to operate in harsh reactor environments, GaN-based semiconductors show promise. Because GaN-based electronics are immature, simple sensor and transmitter circuitry is prioritized to increase the likelihood of success.

This report proposed a robust and simple method of data communication for analog sensors. To test and verify the feasibility of this robust and simple communication method, a robust communications test bed was constructed. Using this test bed, the proposed communication method was implemented and tested using simple commercial off-the-shelf parts.

The proposed simple communication method first encoded an analog voltage from an emulated sensor into a PWM waveform. After encoding, the PWM waveform was then modulated using FSK modulation. The resulting waveform was then transmitted using an ADALM-PLUTO SDR. This process was then repeated for a second emulated sensor using a second SDR.

A single SDR was used to receive the two FSK signals, emulating a base-station hub. The two FSK signals from the two emulated sensors were then individually filtered and shifted down to baseband. Each signal was then demodulated and filtered using a low-pass filter, which recovered the originally transmitted emulated analog voltage. This process was then used to create a series of three tests.

Regarding its efficacy, the three tests demonstrate that emulated voltages transmitted using the proposed communication method can be easily recovered to within approximately 1% to 2% of their true values. Furthermore, the tests demonstrate that large errors occur only occasionally; these errors are directly caused by a changing voltage value and resolve quickly.

5.1 FUTURE WORK

Overall, these tests demonstrate that the proposed communication method is feasible for transmitting and receiving analog voltage values over the air. However, because these three tests were implemented using emulated sensors and transmitters on the robust communications test bed, the next steps necessary in the study of the proposed communication method are (1) to irradiate a set of GaN HEMTs and study their irradiation effects; (2) develop compact circuit models of these devices to design and develop radiation-informed circuitry required for the transmitters; and (3) iteratively fabricate, irradiate the transmitter circuits, and make recommendations for future versions to survive greater TIDs and neutron fluences.

6. REFERENCES

[1] F. K. Reed, N. D. B. Ezell, M. N. Ericson, and C. L. Britton, Jr., "Radiation Hardened Electronics for Reactor Environments," Oak Ridge National Lab.(ORNL), Oak Ridge, TN (United States), Tech. Rep., 2020. [Online]. Available: https://www.osti.gov/biblio/1763473

[2] V. Goiffon, S. Rolando, F. Corbière, S. Rizzolo, A. Chabane, S. Girard, J. Baer, M. Estribeau, P. Magnan, P. Paillet *et al.*, "Radiation Hardening of Digital Color CMOS Camera-on-a-Chip Building Blocks for Multi-MGy Total Ionizing Dose Environments," *IEEE Transactions on Nuclear Science*, vol. 64, no. 1, pp. 45–53, 2016.

[3] M. Menouni, M. Barbero, F. Bompard, S. Bonacini, D. Fougeron, R. Gaglione, A. Rozanov, P. Valerio, and A. Wang, "1-Grad Total Dose Evaluation of 65 nm CMOS Technology for the HL-LHC Upgrades," *Journal of Instrumentation*, vol. 10, no. 05, p. C05009, 2015.

[4] C. Virmontois, V. Goiffon, P. Magnan, S. Girard, C. Inguimbert, S. Petit, G. Rolland, and O. Saint-Pé, "Displacement Damage Effects Due to Neutron and Proton Irradiations on CMOS Image Sensors Manufactured in Deep Submicron Technology," *IEEE Transactions on Nuclear Science*, vol. 57, no. 6, pp. 3101–3108, 2010.

[5] M. J. Gadlage, M. J. Kay, A. R. Duncan, M. W. Savage, J. D. Ingalls, D. Cruz-Rodriguez, and A. Howard, "Impact of Neutron-Induced Displacement Damage on the Multiple Bit Upset Sensitivity of a Bulk CMOS SRAM," *IEEE Transactions on Nuclear Science*, vol. 59, no. 6, pp. 2722–2728, 2012.

[6] J. McGarrity, F. McLean, W. DeLancey, J. Palmour, C. Carter, J. Edmond, and R. Oakley, "Silicon Carbide JFET Radiation Response," *IEEE Transactions on Nuclear Science*, vol. 39, no. 6, pp. 1974–1981, 1992.

[7] D. M. Fleetwood, E. X. Zhang, R. D. Schrimpf, and S. T. Pantelides, "Radiation Effects in AlGaN/GaN HEMTs," *IEEE Transactions on Nuclear Science*, vol. 69, no. 5, pp. 1105–1119, 2022.

[8] C. Witherspoon, F. Reed, M. Ericson, N. Ezell, S. Rajan, R. Cao, A. Balaji, and C. Joishi, "Radiation-hardened gan-based wireless communications architectures for terrestrial nuclear reactor sensing and instrumentation," UT-Battelle, LLC, Oak Ridge, TN, Tech. Rep., 2022.

[9] GNU Radio project, "About gnu radio," https://www.gnuradio.org/about/, 2023, accessed: 2023-06-07.

[10] ——, "Plutosdr source," https://wiki.gnuradio.org/index.php/PlutoSDR_Source, 2023, accessed: 2023-06-14.

[11] AFAR Communications, Inc, "Fcc rules for unlicensed wireless equipment operating in the ism bands," https://afar.net/tutorials/fcc-rules/, 2023, accessed: 2023-06-14.

[12] GNU Radio project, "Simulation example: Fsk," https://wiki.gnuradio.org/index.php/Simulation_example:_FSK, 2023, accessed: 2023-06-14.

[13] ——, "Vco," https://wiki.gnuradio.org/index.php/VCO, 2023, accessed: 2023-06-14.

[14] Tutorials Point India Private Limited, "Frequency shift keying," https://www.tutorialspoint.com/digital_communication/digital_communication_frequency_shift_keying.htm#, 2023, accessed: 2023-06-14.

[15] GNU Radio project, “Quadrature demod,” https://wiki.gnuradio.org/index.php/Quadrature_Demod, 2023, accessed: 2023-06-14.

[16] ——, “Frequency xlating fir filter,” https://wiki.gnuradio.org/index.php/Frequency_Xlating_FIR_Filter, 2023, accessed: 2023-06-14.

[17] ——, “Binary slicer,” https://wiki.gnuradio.org/index.php/Binary_Slicer, 2023, accessed: 2023-06-14.

[18] Robert Keim, “Turn your pwm into a dac,” https://www.allaboutcircuits.com/technical-articles/turn-your-pwm-into-a-dac/, 2016, accessed: 2023-06-14.